OPTICAL LOSS AND HIGH-SPEED MODULATION OF VERTICAL-CAVITY SURFACE-EMITTING LASERS

BY

JANICE T. BLANE

THESIS

Submitted in partial fulfillment of the requirements
for the degree of Master of Science in Electrical and Computer Engineering
in the Graduate College of the
University of Illinois at Urbana-Champaign, 2014

Urbana, Illinois

Adviser:

Professor Kent D. Choquette

Abstract

Vertical-cavity surface-emitting lasers (VCSELs) are microcavity semiconductor lasers used extensively as the light source of short-haul optical data communication and optical interconnects. By increasing the efficiency and modulation speed of these devices, it will be possible to continue to meet a globally increasing demand for bandwidth. After a fundamental discussion of VCSEL design and operation, this thesis focuses on how to improve these microcavity lasers for this type of use. From the collection of light-current-voltage data from lasers with a range of cavity diameters, the effects of varying the impurity doping concentration in the distributed Bragg reflector (DBR) mirrors of the VCSEL on its maximum power, current threshold, and slope efficiency are examined. By optimizing the amount of impurity doping distributed in the mirrors, improved performance of VCSEL can be developed. The small signal modulation theory for semiconductor lasers is also considered. The appropriate equations are derived. Static DC characterizations are conducted on high-speed photonic crystal VCSELs as a next step for determining the characteristics indicative of improved modulation bandwidth.

Acknowledgments

First and foremost, I would like to thank my advisor, Professor Kent Choquette for giving me every opportunity to succeed. His constant support and guidance, intellectual insights, and approachable attitude were what allowed me to complete my thesis. Professor Choquette's enthusiasm to educate, challenge, mentor and care for students is something I intend on taking with me beyond graduate school.

I would also like to thank the former and current members of the Photonic Device Research Group for always being there to answer all of my many questions. I am especially grateful to Gautham Ragunathan, Bradley Thompson, and Zihe Gao for assistance with fabrication, and Tom Fryslie for his time and dedication in helping me with high-speed measurements. It was really a pleasure to be a part of such a fun and cohesive group of people.

Last, but not least, I'd like to thank my family. Without the constant love and support of my parents and my husband, Ben, and the motivation from my son, Braxton, I wouldn't have accomplished so much and be where I am today.

Table of Contents

CHAPTER 1 Introduction
1.1 Background and Motivation…… 1
1.2 Vertical-Cavity Surface-Emitting Laser Operation……2
1.3 Thesis Scope……..... 6
1.4 References……7

CHAPTER 2 VCSELs with Varying Doping Concentrations
2.1 Introduction…… 9
2.2 VCSEL Structure…… 9
2.3 VCSEL Characterization…… 11
2.4 Results……..13
2.5 Discussion……..……19
2.6 References……20

CHAPTER 3 VCSEL Small Signal Modulation
3.1 Introduction……..21
3.2 Theory for Small Signal Modulation in Semiconductor Lasers..…… 21
3.3 VCSEL Structure…… 24
3.4 Static DC Device Characterization……..26
3.5 Summary……..27
3.6 References…….....28

CHAPTER 4 Conclusion
4.1 Summary…….....29
4.2 Future Work……30

Chapter 1
Introduction

1.1 Background and Motivation

Vertical-Cavity Surface-Emitting Lasers (VCSELs) are semiconductor laser diodes that were first devised by Kenicha Iga in 1978 [1]. Since then, they have become the most prominent light source for short-haul optical data communications and optical interconnects, and they are used for many other applications. In the years following their inception, VCSEL operation has developed from pulsed to room-temperature continuous wave operation [2], began operating at lower lasing thresholds due to improved material growth [3], and continue to improve in laser performance with features such as using an oxide aperture [4] which enhances carrier and optical confinement.

VCSELs differ from the traditional edge-emitting lasers in that light emission is perpendicular to the surface of the wafer as opposed to emitting from a cleaved facet. Additionally, they have a circular beam output, low beam divergence, and a small optical mode that facilitates coupling into optical fiber. VCSELs maintain a low operating power and a low threshold current, and can be manufactured at low cost and in high volume. Unlike the edge-emitting laser, which must be cleaved and packaged prior to testing, VCSELs can be probed by on-wafer testing throughout their fabrication process. VCSELs emit in infrared and visible wavelengths, and because of their short cavity length, can operate in a single longitudinal mode. However, because of their relatively broad cross section, they emit into multiple transverse modes as opposed to multiple longitudinal modes.

For the high-speed Internet, the increased demand for bandwidth is becoming a challenge as industry seeks to meet continued expansion and increased functional capability. This has led to the increased use of optical telecommunication and optical data interconnects rather than the conventional electrical interconnect, which suffers from the limitations of cross-talk, frequency dependent losses, and frequency resonance effects [5, 6]. Optical interconnects have less signal degradation, reduced cable bulk,

smaller connectors, and reduced electromagnetic interference. The qualities of the VCSELs have made them the ideal light source for optical data communication, and by pursuing methods to increase the efficiency and modulation bandwidth of these optical devices, it becomes more feasible to meet the bandwidth demands of the future Internet.

1.2 Vertical-Cavity Surface-Emitting Laser Operation

The basic components of a laser consist of a pumping mechanism, a gain medium or optical frequency amplifier, and an optical feedback cavity (typically consisting of two parallel mirrors). In this configuration, the pumping mechanism creates a population inversion within the gain medium such that the amplified light is reflected back and forth within the optical cavity, and when the medium optical gain overcomes the total optical losses within the cavity, the laser achieves the threshold of stimulated emission. For laser diodes, the injection current at which this occurs is called the threshold current.

The VCSEL is an electrically pumped semiconductor laser diode surrounded on either side by highly reflective distributed Bragg reflectors (DBRs) mirrors. Figure 1.1 illustrates the side view of an oxide-confined VCSEL, which is currently the most commonly used device design [4]. On the top and bottom of the wafer are metal contacts to allow for the electrical injection current. The active gain region typically consists of one or more quantum well(s) positioned inside of a p-n junction, and on either side there are the top and bottom n- or p-type DBR mirrors consisting of 20 or more periods of low and high index semiconductor layers [7]. The most commonly manufactured VCSEL emits at nominally 850 nm and is grown on a GaAs substrate. The oxide aperture layers shown in Figure 1.1 are placed near the active region in the DBR mirror in order to guide the injected current into the active region and provide lateral index confinement of the optical mode [4]. Laser emission occurs through the top of the VCSEL, perpendicular to the substrate.

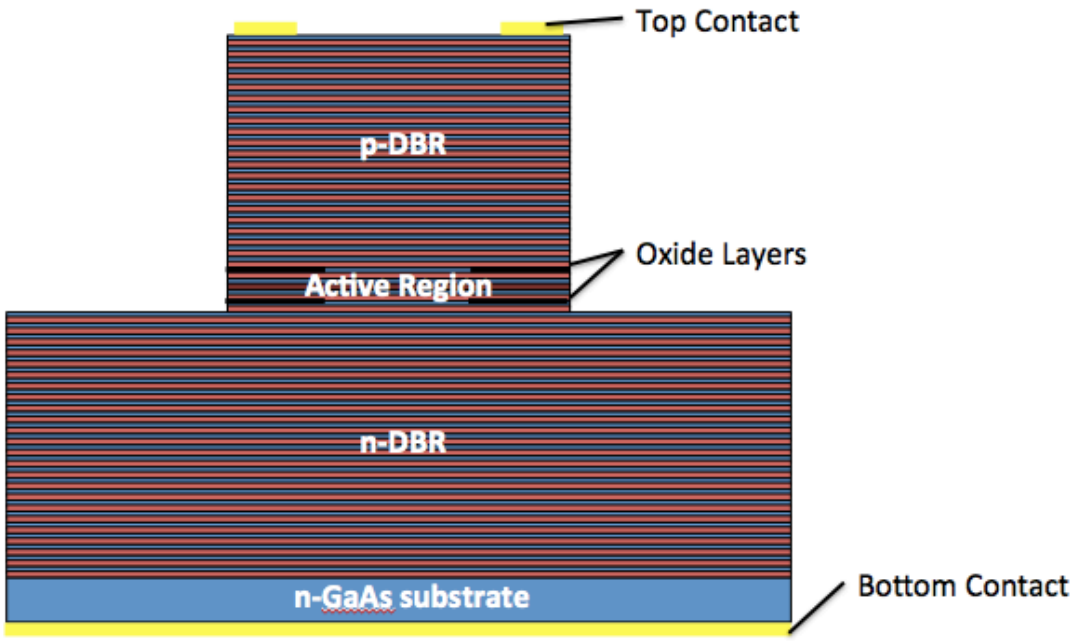

Figure 1.1: Profile of Oxide-Confined VCSEL

As stated earlier, in order to achieve lasing, the optical gain must overcome the total optical losses in the cavity. The losses include light transmitting through the mirrors, as well as light absorbed by the impurities in the doped mirrors. Careful consideration of the layer thicknesses and composition has to be made in the design to ensure that the longitudinal mode profile adequately spatially overlaps the optical gain profile. In the VCSEL, the active medium is located in the intrinsic region of a p-n junction with the semiconductor quantum wells placed at the antinodes of the electromagnetic field in order to achieve optical gain [8]. The requirements for modal threshold gain for the VCSEL is similar to a Fabry-Perot cavity and can be given by [9]

$$\Gamma g_{th} = \alpha + \frac{1}{2L}\ln\left(\frac{1}{R_1 R_2}\right) \tag{1.1}$$

where Γ is the optical confinement factor for both the longitudinal and transverse confinement, g_{th} is the material gain threshold, α is the intrinsic loss, L is the effective cavity length, and R_1 and R_2 are the mirror reflectivities. The first term on the right side of Equation 1.1 is the optical absorption inside the cavity, while the second term is the mirror loss.

The optical feedback cavity used to confine the light within the VCSEL is created by high reflectivity (>99%) DBR mirrors. DBRs are alternating layers of semiconductor or dielectric materials with high and low refractive indices. The high reflectivity for the VCSEL is created by the constructive interference of reflected light from the multiple high/low index interfaces in the DBR mirror. The high reflectivity occurs because the multiple alternating pairs of quarter-wavelength thick high and low refracted index layers are separated by an optical thickness of a multiple of a half-wavelength.

The intensity reflection coefficient of the DBR is given by [10]

$$R = tanh^2\left(\frac{M_B}{2}\left[\frac{n_h}{n_l} - \frac{n_l}{n_h}\right]\right) \tag{1.2}$$

where M_B is the number of periods in the DBR, n_h and n_l is the high and low averaged refractive index of each layer in each period.

Unfortunately, these large differences in refractive index of the semiconductor layers in the mirrors imply conduction and valence band offsets which can impede the flow of electrical injection current used to excite the quantum well, which results in high series resistance. This increased resistance can be overcome by increasing the impurity doping concentration within the DBRs. Excessively high doping is undesirable, however, because of the effects of free-carrier optical absorption [7]. Therefore, in order to reduce the absorption, relatively lower doping concentration should be placed at the maximum points of the optical field in the DBR mirror [11].

The VCSELs characterized in Chapter 2 use oxide-confinement to funnel the current into the laser cavity as sketched in Figure 1.1. Alternatively, ion implantation is another method used for electrical confinement [7] and is employed in the high-speed VCSELs discussed in Chapter 3. Ion implantation is essentially damaging the DBR by ion bombardment, which creates crystal vacancies and typically is done using hydrogen ions. The ions are implanted into the top DBR mirror surrounding the laser cavity making that portion of the mirror nonconductive, creating guided current flow to the active region of the laser. The ion damage typically does not encroach into the active medium. In order to confine the optical mode

of an ion-implanted VCSEL, a thermal lens is usually created. A thermal lens is a thermally induced refractive index gradient, which aids in the guiding of the optical transverse modes [7].

Another method for controlling VCSEL lateral modes is the use of two-dimensional photonic crystals etched into the surface of the VCSEL. The current and optical confinements are then controlled by independent means, the former dictated by the implantation and the latter controlled by the photonic crystal. The photonic crystals in the VCSELs used in this thesis have a single-defect (i.e. single missing hole) placed in the center of a hexagonal hole pattern in order to provide an optical aperture to confine the transverse modes. Advantages of photonic crystals cavities are that they can lower the diffraction loss in implanted VCSELs and create a stable fundamental mode; and the same photonic crystal design can be used for all wavelengths [12-14]. Figure 1.2 shows a scanning electron microscope image of a high-speed photonic crystal VCSEL.

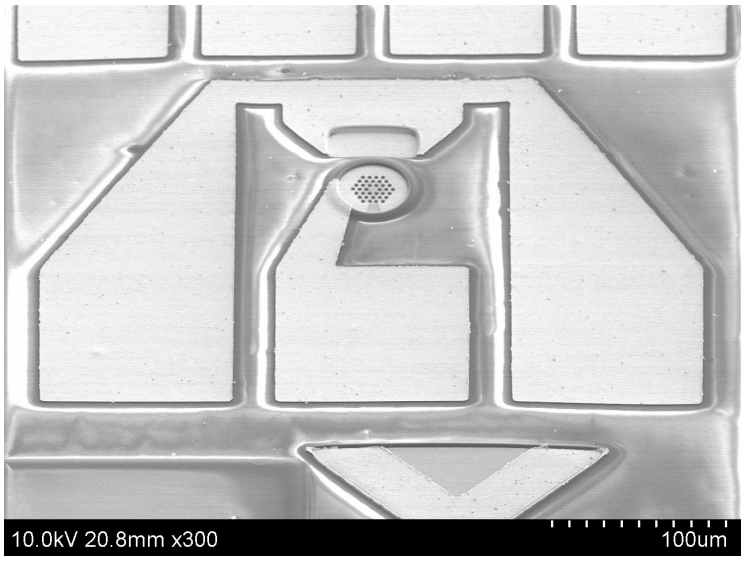

Figure 1.2: Picture of Photonic Crystal VCSEL

Lateral confinement of both the injection current and the optical modes can be simultaneously controlled in oxide-confined VCSELs. The lower refractive index oxide layer is fabricated near the active region to form an aperture. Because the oxide layer is insulating, it minimizes lateral current spreading

outside of the laser cavity and reduces the threshold voltage and current [7, 15]. Optically, the oxide aperture provides index guiding and contributes to the emergence of multiple transverse modes at threshold and the stability of the output beam [7, 16].

1.3 Thesis Scope

The scope of this thesis is to identify improved designs for high-speed modulated VCSELs. This thesis explores using varying doping concentrations in different DBR regions of VCSELs in order to determine the influence on various laser characteristics. This is then followed by the analysis and characterization of photonic crystal VCSELs in order to modulate them at higher frequencies.

Chapter 2 reports the characterization and analysis of the impurity doping concentration in the DBR, which can affect the performance of the VCSELs. First, there is an explanation of the structure of each of the wafers and how each of the wafers differed. Then there is a detailed discussion on the characterization process collecting Light-Current-Voltage (LIV) data for each of the lasers fabricated from the wafers. The data collected from lasers in each wafer spans an oxide aperture diameter range from 0.5 μm to 10 μm. Finally, the experimental results are presented and analyzed by comparing the current thresholds, maximum powers, and slope efficiencies for each of the different doping samples.

Chapter 3 focuses on the small signal modulation of high-speed photonic crystal VCSELs. The chapter begins with the theory for small signal modulation in semiconductor lasers and then discusses the characterization of several high-speed VCSEL devices. The chapter includes a description of the static DC characterization of several of the high-speed devices and presents the results from the collection of LIV data used for determining the optimal lasers to study their small signal modulation performance.

Chapter 4 concludes with a summary of the work presented and discusses the future characterization of high-speed VCSELs.

1.4 References

[1] H. Soda, K. Iga, C. Kitahara, and Y. Suematsu, "GaInAsP/InP surface emitting injection lasers," *Japan Journal of Applied Physics*, vol. 18, pp. 2329–2330, December 1979.

[2] F. Koyama, S. Kinoshita, and K. Iga, "Room-temperature continuous wave lasing characteristics of GaAs vertical cavity surface-emitting laser," *Applied Physics Letters*, vol. 55, no. 3, pp. 221–222, July 1989.

[3] J. L. Jewell, A. Scherer, S. L. McCall, Y. H. Lee, S. Walker, J. P. Harbison, and L. T. Florez,, "Low-threshold electrically pumped vertical-cavity surface-emitting micro-lasers," *Electronics Letters*, vol. 25, pp. 1123-1124, 1989.

[4] K. D. Choquette, R. P. Schneider, Jr., K. L. Lear, and K. M. Geib, "Low threshold voltage vertical-cavity lasers fabricated by selective oxidation," *Electronic Letters*, vol. 30, no. 24, pp. 2043-2044, November 1994.

[5] D. A. B. Miller, "Device requirements for optical interconnects to silicon chips," *Proceedings of the IEEE*, vol. 97, no. 7, pp. 1166-1185, July 2009.

[6] M. A. Taubenblatt, "Optical interconnects for high-performance computing," *Journal of Lightwave Technology*, vol. 30, no. 4, pp. 448-457, February 2012.

[7] K. D. Choquette and K. M. Geib, "Fabrication and performance of vertical-cavity surface-emitting lasers," in *Vertical-Cavity Surface-Emitting Lasers*, Wilmsen, Temkin, and Coldren, Eds., New York: Cambridge, 1999, pp.193-232.

[8] S. W. Corzine, R. S. Geels, et al., "Design of Fabry-Perot surface-emitting lasers with a periodic gain structure," *IEEE Journal of Quantum Electronics*, vol. 25, no. 6., pp. 1513-1524, June 1989.

[9] S. L. Chuang, *Physics of Optoelectronics Devices*. New York: Wiley Interscience, 1995.

[10] K. J. Ebeling, *Integrated Optoelectronics*. Berlin: Springer-Verlag, 1993.

[11] K. Kojima, R. A. Morgan, et al. "Reduction of p-doped mirror electrical resistance of GaAs/AlGaAs vertical-cavity surface-emitting lasers by delta doping," *Electronics Letters*, vol. 29, no. 20, pp. 1771-1772, September 1993.

[12] D. S. Song, S. H. Kim, H. G. Park, C. K. Kim, and Y. H. Lee, "Single-fundamental-mode photonic-crystal vertical-cavity surface-emitting lasers," *Applied Physics Letters*, vol. 80, no. 21, pp. 3901-3903, May 2002.

[13] N. Yokouchi, A. J. Danner, and K. D. Choquette, "Two-dimensional photonic crystal confined vertical-cavity surface emitting lasers," *IEEE Journal of Selected Topics in Quantum Electronics*, vol. 9, pp. 1439-1445, 2003.

[14] A. M. Kasten, M. P. Tan, J. D. Sulkin, P. O. Leisher, and K. D. Choquette, "Photonic crystal vertical cavity lasers with wavelength independent single mode behavior," *IEEE Photonic Technology Letters*, vol. 20, pp. 2010-2012, 2008.

[15] K. D. Choquette, K. L. Lear, R. P. Schneider, and K. M. Geib, "Cavity characteristics of selectively oxidized vertical-cavity lasers," *Applied Physics Letters*, vol. 66, no. 25, pp. 3413-3415, June 1995.

[16] K. L. Lear, R. P. Schneider, Jr., K. D. Choquette, and S. P. Kilcoyne, "Index guiding dependent effects in implant and oxide confined vertical-cavity lasers," *IEEE Photonics Technology Letters*, vol. 8, no. 6, pp. 740-742, June 1996.

Chapter 2

VCSELs with Varying Doping Concentrations

2.1 Introduction

This chapter discusses the effects of varying doping concentrations in distributed Bragg reflector mirrors. It begins with a description of the VCSELs used in the testing, followed by the methods used in the characterization process. Light-Current-Voltage (LIV) data is collected and used to compare the maximum power, current threshold, and slope efficiency for a set of VCSEL wafers that have several different doping schemes employed in their DBR mirrors.

2.2 VCSEL Structure

Seven different VCSEL wafers were grown at Sandia National Labs for comparing the effects of varying doping concentrations in the distributed Bragg reflector mirrors. Using these wafers, VCSELs with varying sized oxide apertures were fabricated by the Photonic Device Research Group at the University of Illinois. These oxide-confined AlGaAs VCSELs emit at approximately 850 nm. The fabricated VCSEL samples contain repeating unit cells of multiple VCSELs. A unit cell consists of two rows of VCSELs with square mesas whose sides vary from 30-44 μm with 0.5 μm step size and two rows of square mesas whose sides vary from 45-75 μm with 1.0 μm step size. Figure 2.1 shows an optical micrograph of a unit cell. Each individual VCSEL is composed of a top p-type DBR with 22 periods, a quarter wavelength thickness oxide on each side of the optical cavity that contains a five quantum well active region, and a bottom n-type DBR with 35 periods. Each period consists of 36 nm of $Al_{0.16}Ga_{0.84}As$, 26 nm of a linear composition grade, 41.7 nm of $Al_{0.94}Ga_{0.06}As$, and another 26 nm of a linear composition grade.

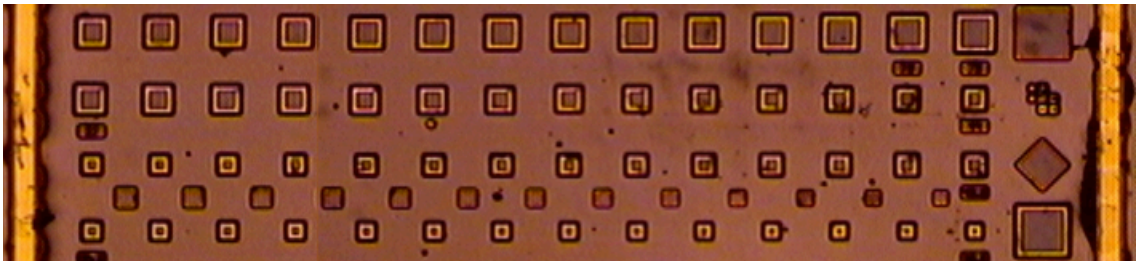

Figure 2.1: Unit Cell of VCSELs with Varying Mesa Sizes

For comparison, the cross-section laser structure was divided into four different doping regions, as sketched in Figure 2.2: the top 20 periods (p-type DBR), the inner top 2 periods (p-type DBR), the inner bottom 2 periods (n-type DBR), and the bottom 33 periods (n-type DBR). Each of the different doping regions has either high (4×10^{18} cm^{-3}), mid (2×10^{18} cm^{-3}), or low (5×10^{17} cm^{-3}) doping concentrations of n-type (Si) or p-type (C) dopants. Table 2.1 presents the intended doping concentration for the various regions as well as the measured lasing wavelengths for each of the wafers.

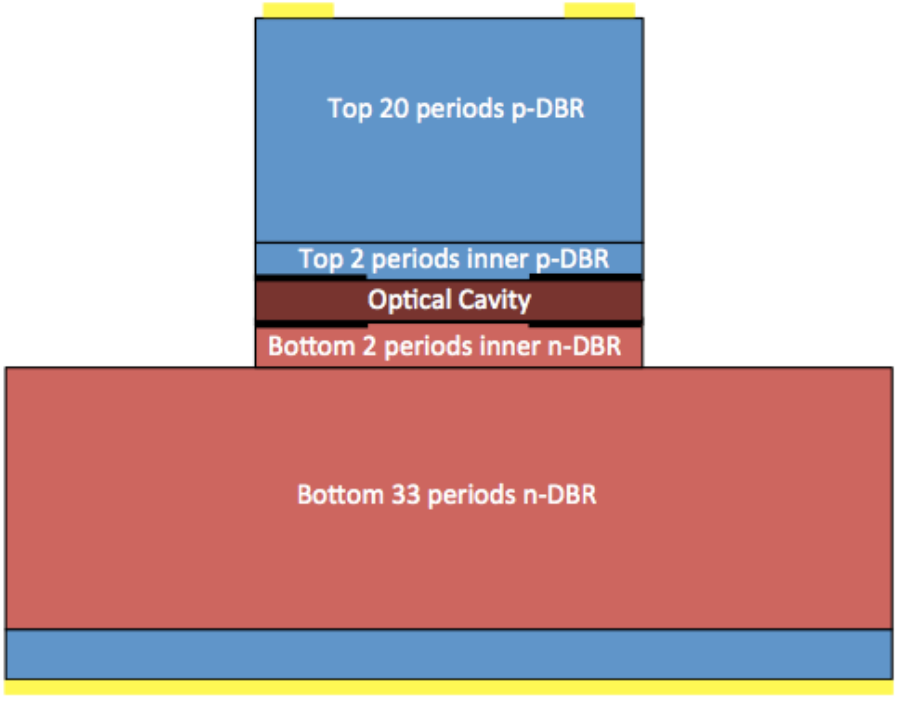

Figure 2.2: Device Structure Profile Showing the Regions of Varying Impurity Concentration

Table 2.1: Description of the VCSEL Wafers

Structure	EMC1000	EMC1001	EMC1003	EMC1004	EMC1005	EMC1006	EMC1007
Top 20 period p-DBR	4.0 E18 high	4.0 E18 high	4.0 E18 high	4.0 E18 high	4.0 E18 high	4.0 E18 high	2.0 E18 mid
Top 2 periods inner p-DBR	2.0 E18 mid	2.0 E18 mid	2.0 E18 mid	2.0 E18 mid	4.0 E18 high	5.0 E17 low	2.0 E18 mid
oxide layer Optical cavity: 5 QWs oxide layer							
Bottom 2 period inner n-DBR	1.5 E18 mid	3.0 E18 high	1.5 E18 mid	5.0 E17 low	1.5 E18 mid	1.5 E18 mid	1.5 E18 mid
Bottom 33 period n-DBR	2.0 E18 mid	3.0 E18 high	3.0 E18 high	3.0 E18 high	3.0 E18 high	3.0 E18 high	3.0 E18 high
Fabry-Perot wavelength	849	844	848	846	846	847	850

2.3 VCSEL Characterization

An analysis of each wafer was performed through a characterization procedure that measured voltage and light output versus injected current for VCSELs in each of the wafers. The Light-Current-Voltage (LIV) characteristics are useful for determining the current threshold, maximum power, and slope efficiency properties of an individual VCSEL. By measuring these parameters as a function of the laser diameter, the effects of the various doping schemes can be evaluated.

The main components for the testing apparatus consists of an ALESSI probe station with a broad area Si photodetector, an Agilent Precision Semiconductor Parameter Analyzer (SPA), Yokogawa AQ 6370C Optical Spectrum Analyzer (OSA), a Keithley 236 DC power supply, and a LabVIEW program operating on a computer that interfaces with the SPA. A block diagram and picture of the setup is shown in Figure 2.3 (a) and (b), respectively.

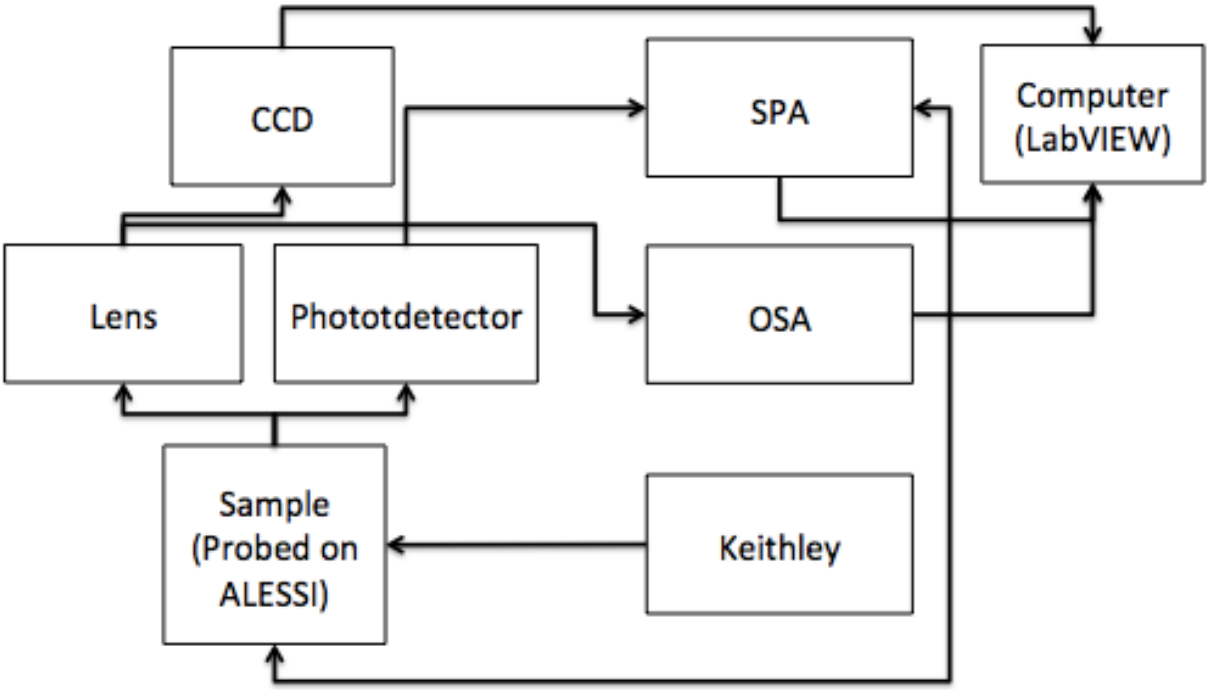

(a)

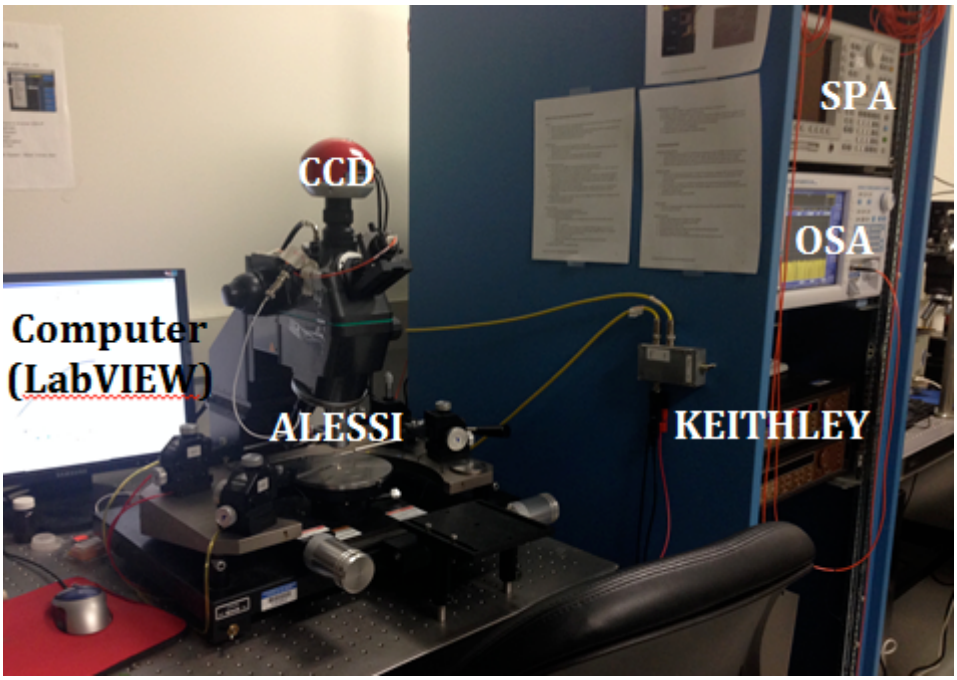

(b)

Figure 2.3: VCSEL Characterization Setup: (a) Block Diagram and (b) Picture Showing the Equipment Used

In the first part of the laser characterization process, the VCSEL sample is placed on the probe station and is operated by the DC power supply. The lasing wavelength above but near threshold is then measured by the Optical Spectrum Analyzer using an optical fiber that images the VCSEL emission from the probe station. Once the lasing wavelength is determined, a corresponding responsivity value for the photodetector is used by the LabVIEW program for calibrated optical output power measurements. In the next part of the characterization process, the VCSEL power supply is switched to the SPA and the photodetector is placed directly above the VCSEL. The start, stop, and step size of the injection current are input parameters for the LabVIEW program in order for the system to measure LIV data for the sample under testing. Figure 2.4 shows typical LIV data extracted from the VCSELs studied in this work.

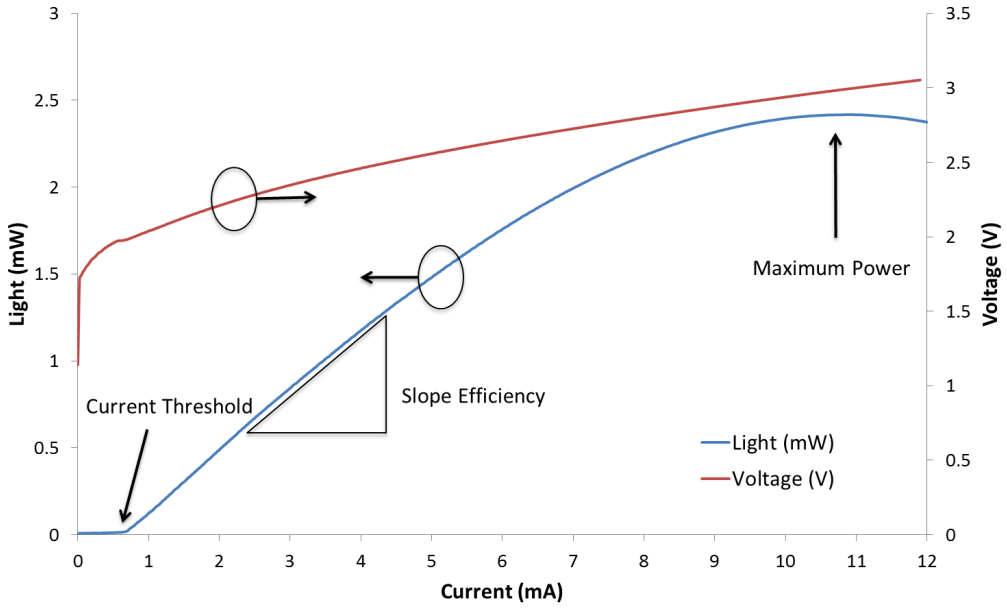

Figure 2.4: Typical LIV Characteristics of 5 x 5 μm^2 Oxide Aperture VCSEL (1003)

2.4 Results

Three device parameters are extracted from the LIV data for comparison of VCSELs with varying doping concentrations: maximum output power, lasing threshold, and the laser output slope efficiency.

Devices from one unit cell of each wafer are measured. For each unit cell, VCSELs with square mesa sides of length 0.5 - 10 μm are characterized.

Specific methods are used to extract the different characteristics from the measured LIV data as shown in Figure 2.4. Maximum output power occurs at the "rollover injection current" as determined by the LI curve. The current threshold is the current where stimulated emission begins to dominate over spontaneous emission, and is indicated by dramatic increase of optical output, as shown in Figure 2.4. Finally, the laser slope efficiency is found from the slope of the linear portion of the LI curve beyond the current threshold and prior to the rollover current. In the following, we compare these three parameters versus device size and doping variations. In some cases, no identifiable trend can be observed in the comparisons; hence, we present only the parameters showing significant differences.

The first comparison is conducted to determine the effects of varying the doping concentrations for the top 20 periods p-DBRs of the VCSEL. Sample 1003, which has high doping in this region, and sample 1007, which differs only with a medium doping in this region, are compared. The only significant difference between the two samples is observed in the current threshold comparison. As seen in Figure 2.5 for both wafers, larger diameter VCSELs have a higher threshold current than smaller diameters, except for the smallest devices. This is in agreement with prior reports [1]. Note that the higher threshold current density for the smallest VCSEL sizes (below 3 μm) is due to the increased diffraction loss in smaller apertures [1]. As shown in Figure 2.5, the higher doped sample had an overall lower current threshold across the varying aperture sizes. The lower threshold current is surprising due to its higher doping concentration, which should be accompanied by the higher optical loss [2].

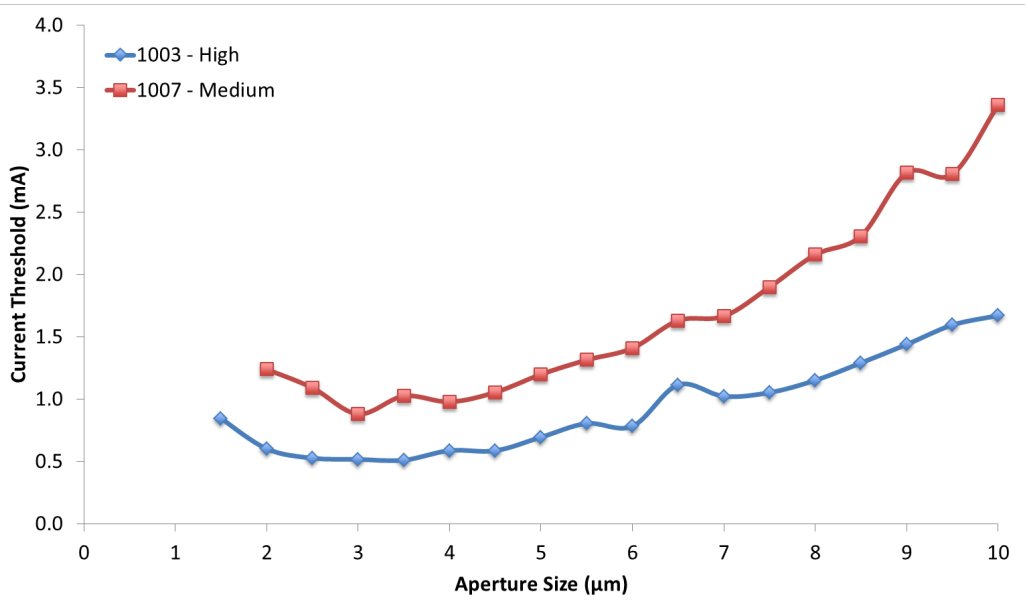

Figure 2.5: VCSEL Top 20 Periods p-DBR Comparison (Current Threshold)

The second comparison considers the different doping concentrations for the top 2 inner p-DBR periods of the VCSELs. Samples 1005 (high doping), 1003 (medium doping), and 1006 (low doping) are examined. Differences are observed in comparisons between the maximum power and slope efficiency. Figure 2.6 (a) shows the differences in maximum power versus cavity size between the three VCSEL samples. As expected, the maximum power increases with an increasing injection current. The samples with lower doping in the innermost 2 DBR periods have a higher maximum power for a given injection current level. Figure 2.6 (b) shows the slope efficiencies of these samples. At the smallest aperture sizes, the slope efficiency is extremely low, but at approximately 1-2 µm diameter, the slope efficiency increases dramatically followed by saturation for devices with an oxide aperture greater than approximately 4 x 4 μm^2. The devices with the lowest doping tend to have the higher slope efficiency for a given cavity size.

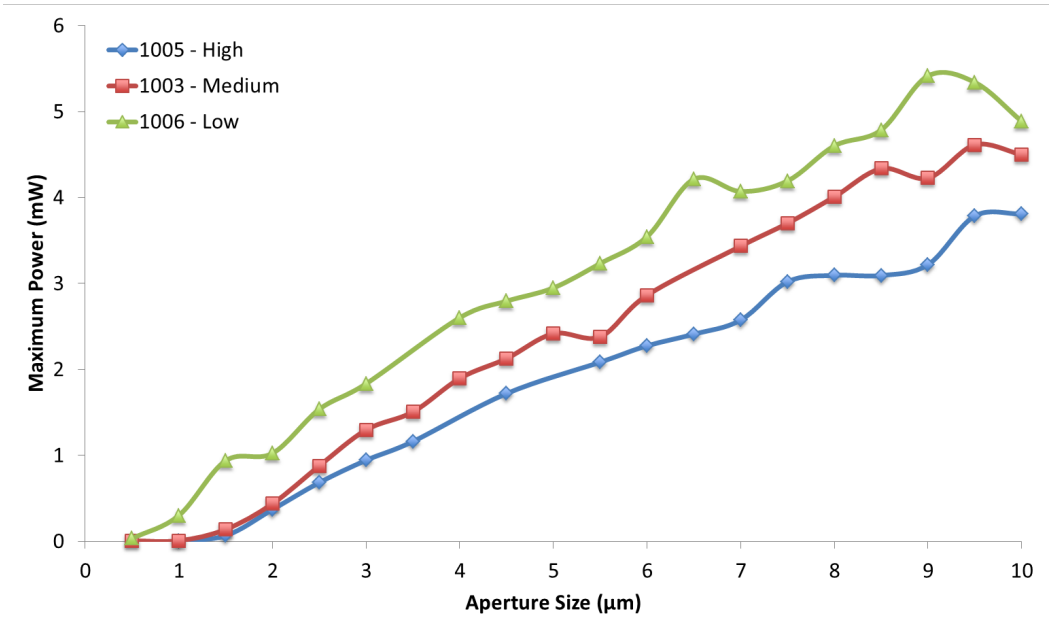

(a)

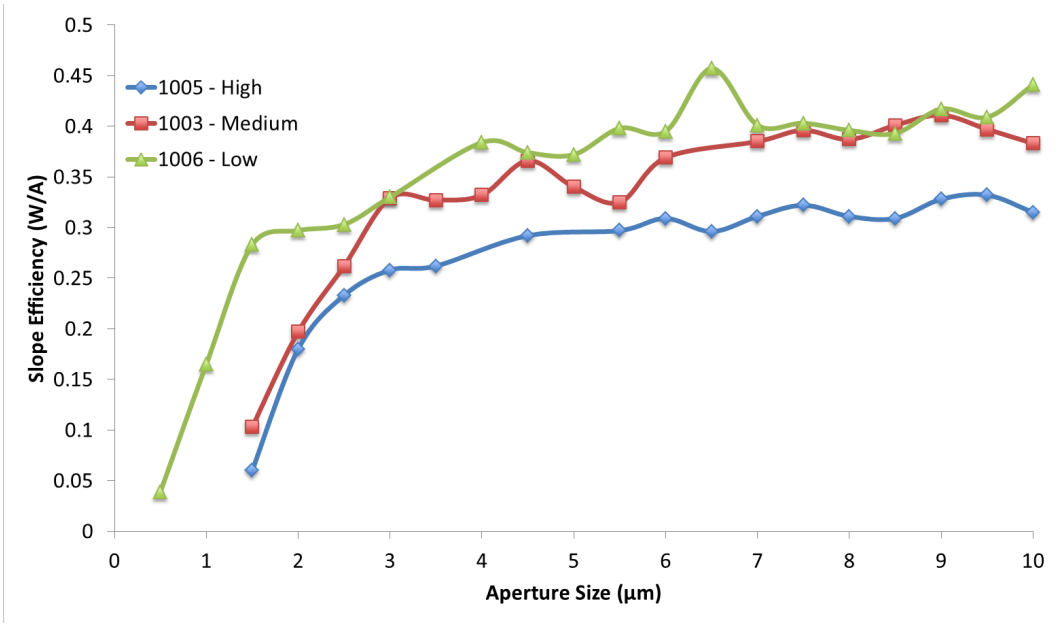

(b)

Figures 2.6: VCSEL Top 2 Periods Inner p-DBR Comparison: (a) Maximum Power and (b) Slope Efficiency

The next comparison is between samples with varying bottom inner 2 periods of the n-type DBRs. The samples used in this comparison were 1001 (high doping) and 1003 (medium doping). These two wafers only varied in slope efficiency. Figure 2.7 plots the slope efficiency for the VCSELs. The slope efficiency for these VCSELs increase in a similar manner as the devices in Figure 2.6, and above 2 μm size, the VCSELs with the lower doping in this region have the higher slope efficiency, also similar to Figure 2.6.

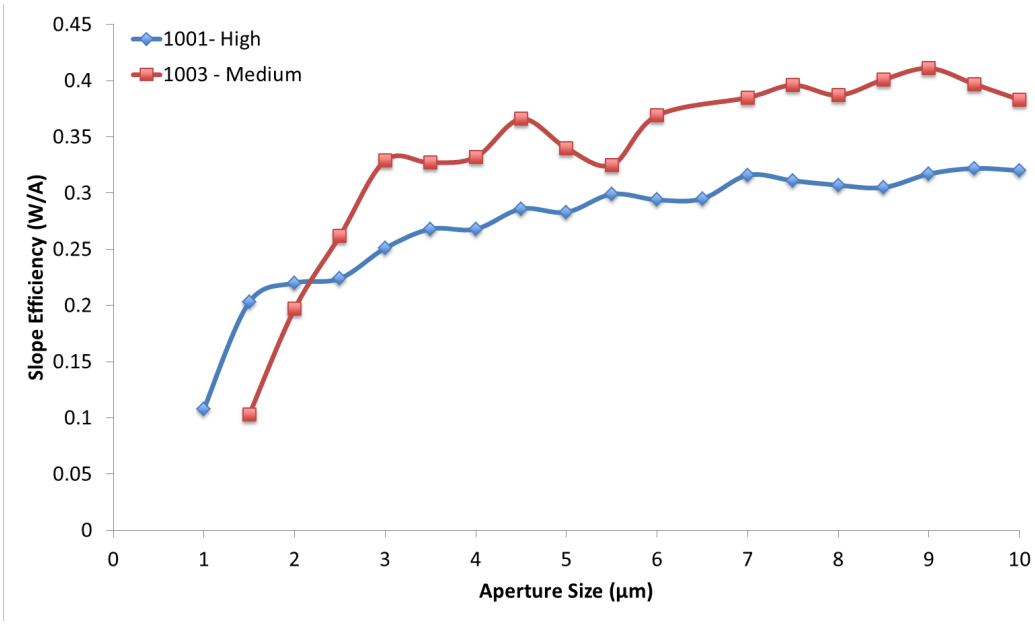

Figure 2.7. VCSEL Bottom 2 Periods Inner n-dBR Comparison (Slope Efficiency)

Finally, the set of VCSELs with varying bottom 33 periods of the n-type DBR are compared. The samples compared are 1003 (high doping) and 1000 (medium doping). Maximum power, current threshold, and slope efficiency all differed between these wafers. Figure 2.8 (a) shows the increasing maximum power with increasing aperture size for the VCSELs. Similar to Figure 2.6 (a), the VCSELs with the lower doping in this region had higher maximum power for a given aperture size. In Figure 2.8 (b), the threshold current of the VCSELs is compared. Similar to Figure 2.5, the higher doped VCSELs tended to have the lower threshold. Finally, the slope efficiencies are compared in Figure 2.8 (c). The

curves show the same trends as Figures 2.6 (b) and 2.7, where as seen before, the VCSELs with the lower doping have the highest slope efficiencies.

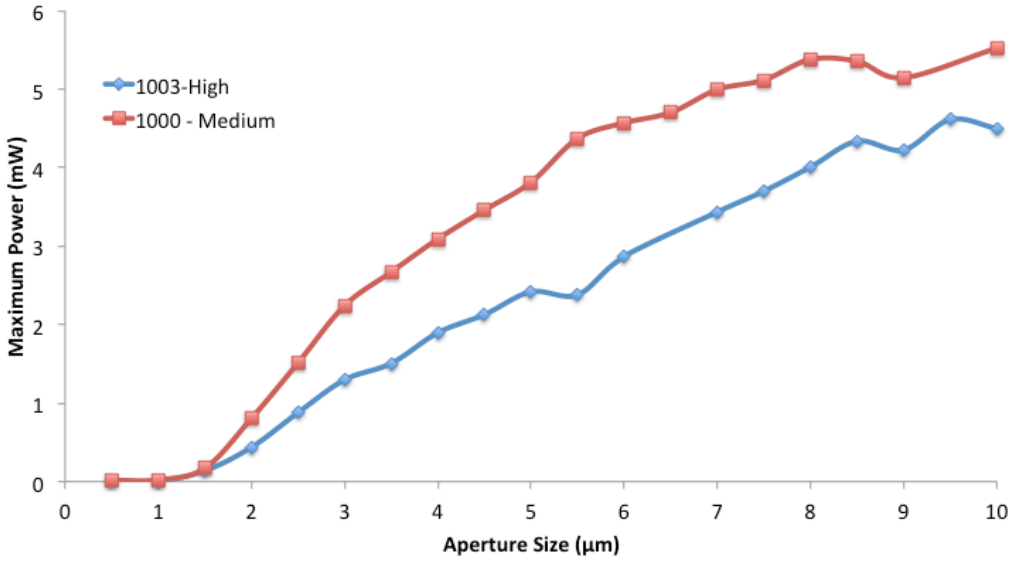

(a)

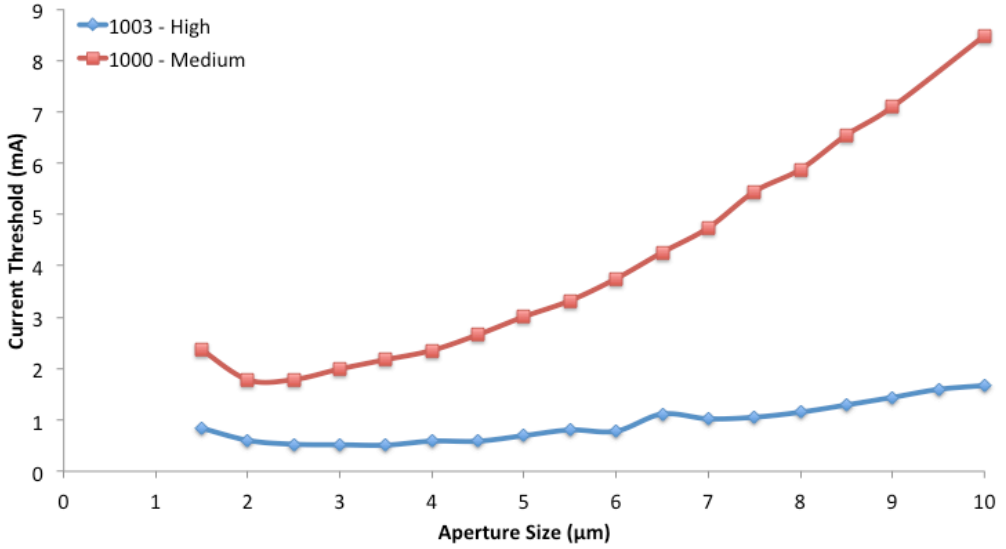

(b)

Figure 2.8: VCSEL Bottom 33 Periods n-DBR Comparison (a) Maximum Power (b) Current Threshold and (c) Slope Efficiency

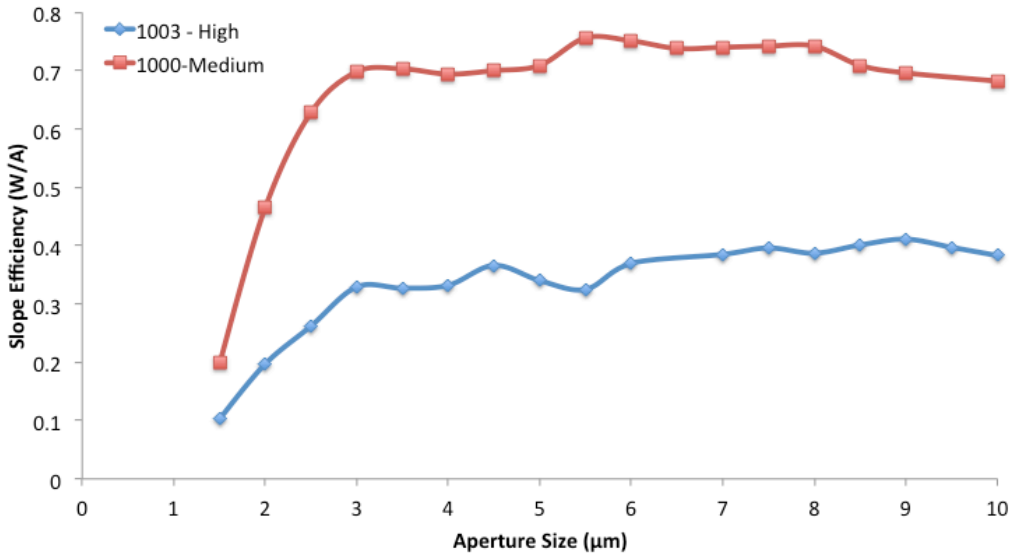

(c)

Figure 2.8: Continued.

2.5 Discussion

This chapter has a focus on examining the effects of the varying of doping concentrations in different DBR regions within the VCSELs. Shown in Figure 2.9 is the optical standing wave and the refractive index profile of the VCSELs. Notice the longitudinal optical mode has greater overlap, and hence more absorption, with impurities in the innermost 2 periods next to the optical cavity. Therefore, the results in Figures 2.6 (b), 2.7, and 2.8 (c), which show higher slope efficiency for lower impurity concentrations are consistent with less absorption. Greater slope efficiency is also consistent with greater output power, as indicated by Figures 2.6 (a) and 2.8 (a). However, lowest threshold current occurring for the higher doped samples is not consistent, unless mirror loss of these lasers dominates the required optical gain (see Equation 1.1). We conclude that a combination of lower doping in the top 20 periods p-DBR and lower doping in the top 2 periods inner p-DBR yields the best performance for maximum power, current threshold, and slope efficiency.

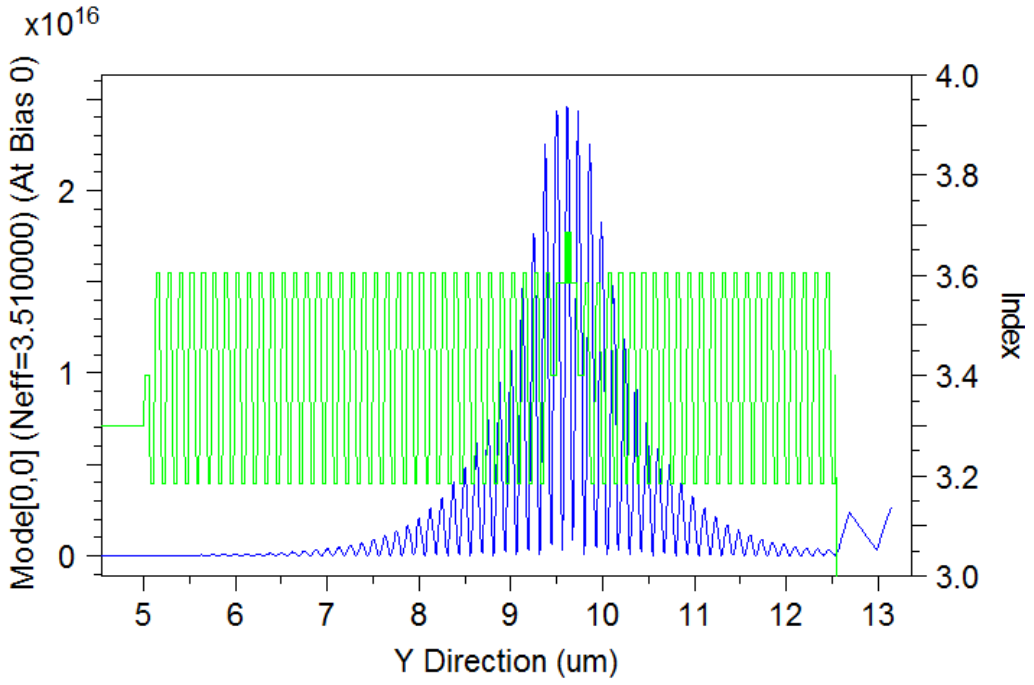

Figure 2.9: Intensity Standing Wave and Refractive Index Profile of VCSELs

2.6 References

[1] K. D. Choquette, W. W. Chow, G. R. Hadley, H. Q. Hou, and K. M. Geib, "Scalability of small-aperture selectively oxidized vertical-cavity lasers," *Applied Physics Letters*, vol. 70, no. 7, pp. 823-825, February 1997.

[2] K. D. Choquette and K. M. Geib, "Fabrication and performance of vertical-cavity surface-emitting lasers," in *Vertical-Cavity Surface-Emitting Lasers*, Wilmsen, Temkin, and Coldren, Eds., New York: Cambridge, 1999, pp.193-232.

Chapter 3

VCSEL Small Signal Modulation

3.1 Introduction

Intensity modulation of VCSELs is extensively used in optical interconnect applications. A popular technique to characterize intensity modulation in semiconductor lasers is called small signal modulation. This chapter discusses small signal modulation in VCSELs. It begins with an explanation of the theory for semiconductor lasers, which establishes the foundation for small signal testing and predicts the expected results. This is then followed by a description of the VCSELs used during testing and results are reported from static DC device characterization. Based on the DC testing, devices could then be selected for future characterization in small signal modulation.

3.2 Theory for Small Signal Modulation in Semiconductor Lasers

In semiconductor lasers, the output light power intensity increases approximately linearly with injection current above threshold, as seen in Figure 2.4. Thus, an injection current with a DC component and a small signal AC modulation at some frequency would therefore result in constant output light power intensity with a corresponding small signal variation of intensity at the same frequency.

For a single mode laser, the differential rate equations for carrier density and photon density are used to describe how the laser responds to these small dynamic changes from their steady-state values [1]:

$$\frac{dn(t)}{dt} = \eta_i \frac{J(t)}{qd} - \frac{n(t)}{\tau} - v_g g(n) S(t) \tag{3.1}$$

$$\frac{dS(t)}{dt} = \Gamma v_g g(n) S(t) - \frac{S}{\tau_p} + \beta R_{sp}(n) \tag{3.2}$$

where $n(t)$ is the electron density (cm^{-3}), η_i is the injection quantum efficiency, q is the unit charge (C), τ is the carrier lifetime (s), v_g is the group velocity of light (cm/s), Γ is the optical confinement factor, $R_{sp}(n)$ is the spontaneous emission rate per unit volume ($cm^{-3}s^{-1}$), $S(t)$ is the photon density (cm^{-3}), $J(t)$ is the injection current density (A/cm^2), d is the thickness of the active region emitting light, τ_p is the photon lifetime (s), $g(n)$ is the gain coefficient (cm^{-1}), and β is the spontaneous emission factor.

In Equation 3.1, the carrier density rate equation, the first term is the injected number of carriers into the active region per unit volume per second; the second term is the carrier loss due to radiative and nonradiative recombinations; and the last term is carrier loss due to stimulated emission. In Equation 3.2, the photon density rate equation, the first term is the increasing rate of the number of photons per unit volume due to the stimulated emission; the second term is the decreasing rate of the photon density due to intrinsic absorption losses; and the third term is the fraction of spontaneous emission entering the lasing mode.

A simplified nonlinear gain coefficient can be used in Equation 3.1 and 3.2:

$$g(n,S) = \frac{g(n_0) + g'(n(t) - n_0)}{1 + \epsilon S(t)} \tag{3.3}$$

where n_0 is the steady-state carrier density, g' is the differential gain, and $1 + \varepsilon S$ accounts for nonlinear gain saturation [1]. Then

$$J(t) = J_0 + j(t) \tag{3.4a}$$

$$n(t) = n_0 + \Delta n(t) \tag{3.4b}$$

$$S(t) = S_0 + s(t) \tag{3.4c}$$

are assumed where J_0, n_0, and S_0 are the DC terms with $j(t)$, $\Delta n(t)$, and $s(t)$ as the corresponding frequency dependent terms, respectively.

Assuming a sinusoidal small signal with angular momentum ω, phasor notation is used in the frequency domain

$$j(t) = Re[j(\omega)e^{-i\omega t}] \tag{3.5a}$$

$$\Delta n(t) = Re\left[\Delta n(\omega)e^{-i\omega t}\right] \tag{3.5b}$$

$$s(t) = Re[s(\omega)e^{-i\omega t}] \tag{3.5a}$$

The steady-state solutions can then be determined by substituting Equations 3.4 and 3.5 into the rate equations, Equations 3.1 and 3.2. Then by solving for s(ω) and dividing by j(ω), the small signal modulation response function is derived

$$M(\omega) = \frac{s(\omega)}{j(\omega)} = \frac{(\frac{\eta_i \Gamma \tau_p}{qd})\omega_r^s}{\omega_r^2 - \omega^2 - i\gamma\omega} \tag{3.6}$$

where $f_r = \omega_r/2\pi$ is the relaxation oscillation frequency given as

$$f_r \cong \frac{1}{2\pi}\sqrt{\frac{v_g g' S_0}{\tau_p(1+\epsilon S_0)}} \tag{3.7}$$

and the damping rate γ is given as

$$\gamma \cong \frac{1}{\tau} + K f_r^2 \tag{3.8}$$

where a K factor (ns) is defined as

$$K = 4\pi^2(\tau_p + \frac{\epsilon}{v_g g'}) \tag{3.9}$$

The 3-dB cutoff frequency, which is used to define the small signal bandwidth of a laser, is defined as the frequency where the modulation bandwidth decreases to half the DC value. This occurs when

$$2\omega_r^2 = \gamma^2 \cong K^2 f_r^4 \tag{3.10}$$

The maximum relaxation frequency occurs at

$$f_{r,max} = \frac{2\pi\sqrt{2}}{K} \tag{3.11}$$

To increase the VCSEL bandwidth, we desire a high relaxation oscillation frequency. Note from Equations 3.7 and 3.9 that this usually implies an as small of a photon lifetime as possible (controlled by the cavity design), as well as a large differential gain (determined by quantum well material design). In addition, the relaxation oscillation frequency can be increased by increasing the photon density

3.3 VCSEL Structure

High-speed photonic crystal VCSELs (wafer VIS-118B) designed and fabricated at the University of Illinois are used in this work [2, 3]. As opposed to the oxide-confined samples studied in Chapter 2, these lasers use ion implantation to confine the injection current. The lasing wavelength is approximately 850 nm.

The photonic crystal etched into the top facet is the defining characteristic of these VCSELs. The hole pattern has a hexagonal design with a single defect as shown in Figure 3.1. Each unit cell on the wafer consists of 10 rows of VCSELs with 31 to 42 µm mesa sizes. The first column of each of the rows is a control VCSEL without a photonic crystal. The remaining columns consist of identical sets of photonic crystal VCSELs. Figure 3.2 illustrates the layout for the unit cell. How each row differs in design characteristics is detailed in Table 3.1.

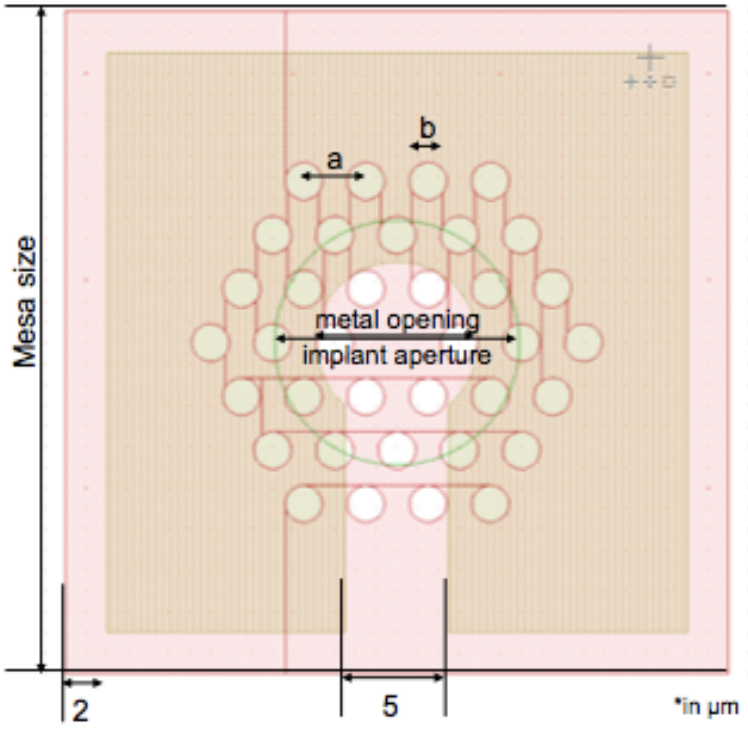

Figure 3.1: Top View Sketch of Photonic Crystal VCSEL

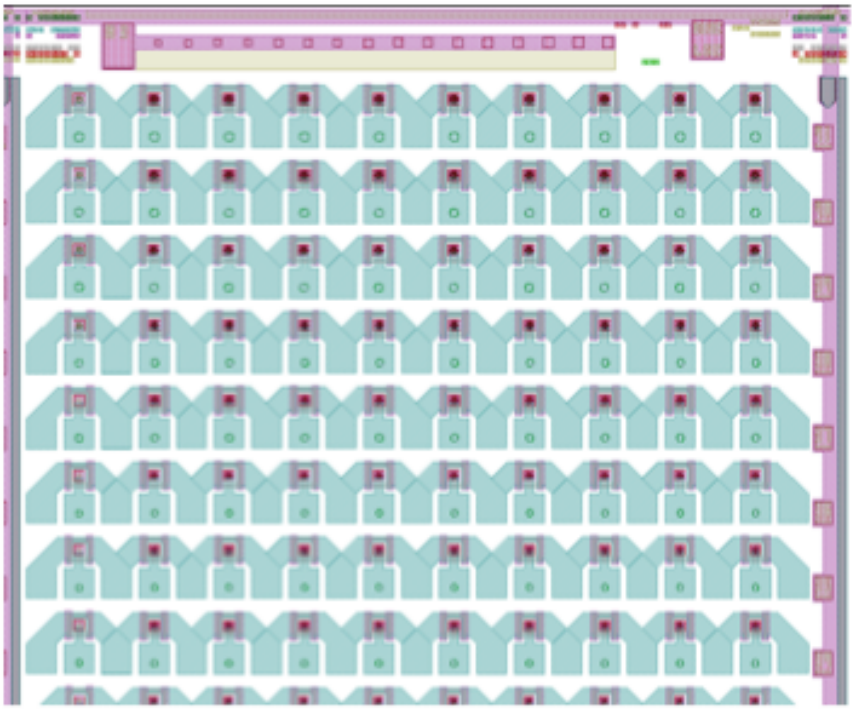

Figure 3.2: Unit Cell Layout

Table 3.1: Design Parameters for Each Row of Unit Cell

Row	b/a	a	b (μm)	metal opening*	implant aperture*	mesa size*
1	0.6	5	3	13	17	41
2	0.7	4.5	3.15	12.15	16.15	40
3	0.6	4.5	2.7	11.7	15.7	39
4	0.7	4	2.8	10.8	14.8	38
5	0.6	4	2.4	10.4	14.4	37
6	0.7	3.5	2.45	9.45	13.45	36
7	0.6	3.5	2.1	9.1	13.1	35
8	0.5	3.5	1.75	8.75	12.75	34
9	0.7	3	2.1	8.1	12.1	33
10	0.6	3	1.8	7.8	11.8	32

* Diameters, in μm

3.4 Static DC Device Characterization

The purpose of static LIV characterization of VCSELs is to screen the multiple photonic crystal designs to focus on the most promising lasers for small signal modulation. The DC device characterization process is identical to the one used in Section 2.3. LIV data is collected for each of the different photonic crystal VCSELs in a unit cell in order to examine the performance of each of the devices. The better performing devices as defined in the following could then be selected for small signal modulation testing.

The first characterization is to ensure that the lasers were functional. Several of the VCSEL designs did not operate, while some devices exhibited dramatic variation compared to others in their rows as far as current threshold or power; and some entire rows (rows 8 and 10) produced light data that was erratic.

The next step was to analyze the LIV data of usable VCSELs in order to determine the highest ratio of injected current at rollover to threshold current (I/I_{th}). Recalling Equation 3.7, a higher ratio should produce a higher modulation bandwidth as the increased current yields an increase in photon density. Devices in row 1 (17 μm implant size) had overall the largest I/I_{th} ratio. Figure 3.3 depicts the LIV data for a VCSEL device in this row. The light-current curve shows a typical bell-type shape with a current threshold at 1.32 mA and a rollover current at 18 mA with a maximum output light of 2 mW. This results in an I/I_{th} ratio of nearly 14. The current-voltage curve increases linearly beyond threshold.

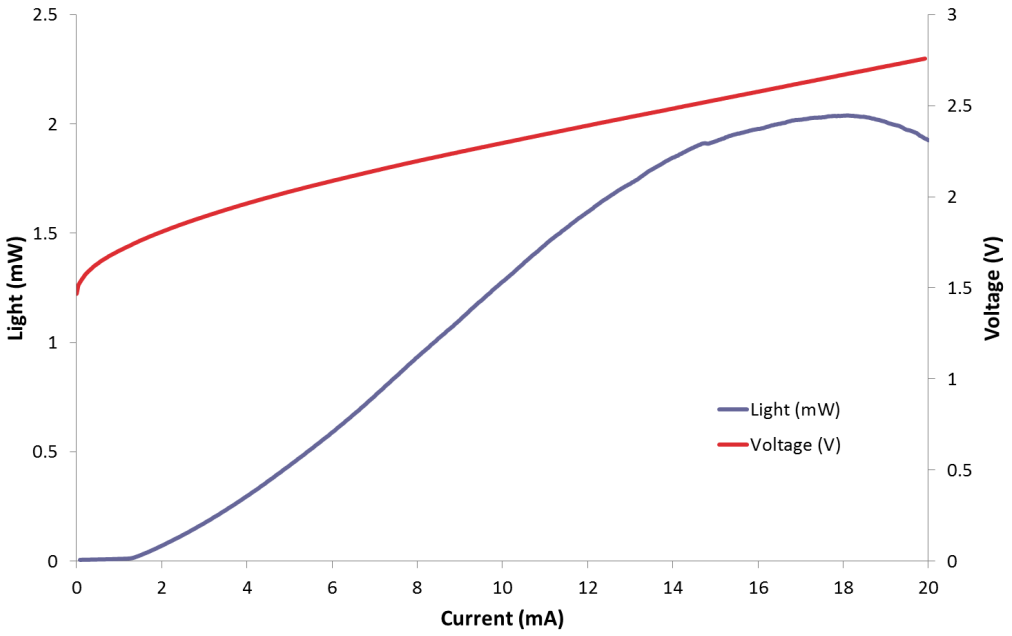

Figure 3.3: VS-118B LIV (Row 1, 17 µm Implant Size)

As apparent in Figure 3.3, a relatively small threshold current with a high rollover current from a VCSEL implies the greatest photon density can be obtained. From Equation 3.7, it can be seen that high photon density should produce the highest relaxation oscillation frequency, leading to the maximum bandwidth. The use of photonic crystal is meant to reduce the number of lasing modes, ideally down to a single mode. The device in Figure 3.3 operates multi-mode, but with far fewer modes than a VCSEL with just an implant aperture [3].

3.5 Summary

In this chapter, the semiconductor laser theory for small signal modulation was examined and used as the foundation for selection of VCSELs with improved modulation properties. After static DC characterizations and deriving the I/Ith ratio, the high-speed photonic crystal VCSELs in row 1 of the unit cell on the wafer sample showed the most promise for producing higher 3-dB bandwidth frequencies.

3.6 References

[1] S. L. Chuang, *Physics of Optoelectronics Devices*. New York: Wiley Interscience, 1995.

[2] M. P. Tan, S. T. M. Fryslie, J. A. Lott, N. N. Ledentsov, D. Bimberg, and K. D. Choquette, "Error-free transmission over 1-km OM4 multimode fiber at 25 Gb/s using a single mode photonic crystal vertical-cavity surface-emitting laser," *IEEE Photonics Technology Letters*, vol. 25, no. 18, pp. 1823-1825, September 2013.

[3] M. P. Tan, S. T. M. Fryslie, J. K. Guenter, J. A. Tatum, R. H. Johnson, K. D. Choquette, "Photonic crystal VCSELs with narrow spectral width and high bandwidth operating at low current density," *Electronic Letters*, vol. 49, no. 9, pp. 612-613, April 2013.

Chapter 4

Conclusion

4.1 Summary

In this thesis, characterization is conducted on oxide-confined and photonic crystal VCSELs. The characterizations on the oxide-confined VCSELs are conducted in order to determine the effects of varying the doping concentrations in different DBR regions of the device on the maximum output power, current threshold, and slope efficiency. The photonic crystal VCSEL characterization include DC static measurements, which consist of analyzing LIV characteristics to determine the best devices for testing the small signal modulation behavior of the devices.

The results for the oxide-confined VCSEL testing compare impurity doping in different regions of the VCSELs at high, medium, or low doping concentrations. A combination of higher doping in the top 20 periods p-DBR and lower doping in the top 2 periods inner p-DBR yields the best performance for greatest power, lowest current threshold, and highest slope efficiency. Furthermore, the lowest I_{th} produces the largest I/I_{th} ratio, which means a greater 3-dB bandwidth.

Chapter 3 discussed small signal modulation theory and presented the LIV results for the DC characterization of several high-speed photonic crystal VCSELs. The devices with the highest I/I_{th} ratio were determined from the data. The highest ratio VCSELs are the VCSELs in row 1 of Table 3.1. This is important because the increased photon flux created in a device with a higher I/I_{th} ratio yields operation at higher modulation bandwidths. This photonic crystal design should then be used for small signal modulation testing.

4.2 Future Work

Vertical-cavity surface-emitting lasers are the dominate technology for the light source of short-haul fiber optic based telecommunication and optical interconnects. This work has shown that varying the doping regions of the VCSELs is one aspect to produce better laser performance, and combined with further study on high-speed modulation, can yield improvement in these and other types of applications. The demand for power and bandwidth will only continue to escalate, and continued VCSEL research will ensure that this demand is met.